

SOURCE MECHANISM DETERMINATION OF LOW MAGNITUDE EARTHQUAKES AND DERIVATION OF THE EASTERN AFRICAN STRESS PATTERN

Andreas Barth¹ and Friedemann Wenzel²

¹ *Heidelberg Academy of Sciences and Humanities; University of Karlsruhe, Geophysical Institute, andreas.barth@gpi.uni-karlsruhe.de*

² *University of Karlsruhe, Geophysical Institute, friedemann.wenzel@gpi.uni-karlsruhe.de*

ABSTRACT

The World Stress Map (WSM) database is a global compilation of recent tectonic stress from a wide range of stress indicators. Earthquake focal mechanisms are the main source to obtain stress data for the WSM. Globally, for most of the stronger earthquakes ($M_w > 5.5$) focal mechanisms are routinely given by Harvard CMT-solutions. However, for the numerous earthquakes of smaller magnitude focal mechanism solutions are hardly available.

We developed a semi-automatic and frequency sensitive moment tensor inversion that allows us to determine source mechanisms of magnitudes $M_w < 5.5$. For the case study of eastern Africa we present focal mechanisms of 38 earthquakes with magnitudes of M_w 4.4-5.5 that occurred between 1995 and 2002 and were not studied previously. We invert data of the permanent global seismometer network with source-receiver distances up to 3300 km within variable frequency bands between 10 mHz and 29 mHz. Since we use a one-dimensional earth model to calculate synthetic waveforms, the method is easily transferable to other regions worldwide and thus can improve the understanding of regional tectonics and give valuable information for seismic hazard assessment.

We combine these new results with all 90 CMT-solutions available for eastern Africa (1977-2005) and 17 focal mechanisms determined by moment tensor inversion from other authors to perform a stress inversion for ten separate areas, that are adopted from the Global Seismic Hazard Assessment Program (GSHAP) and adapted to our data distribution. All over eastern Africa we obtain stable stress tensors, that show a general East-West extension, most likely explained by the effect of gravitational potential energy differences. Regional deviations from this pattern are probably related to the existence of two distinct microplates that are located between the eastern and western rift branch.

INTRODUCTION

The WSM is a compilation of stress orientations of different indicators on different scales. Stress information is deduced from earthquake focal mechanisms, well bore breakouts, drilling-induced fractures, in-situ measurements (hydraulic fracturing, overcoring data and borehole slotter), strain relief measurements and young geological data (Heidbach et al., 2004). The aim of the WSM is to provide standardised and quality-ranked stress data on a world wide scale and to combine different data resources on a user-friendly and online available database (<http://www.world-stress-map.org>). The major part of the WSM stress data, however, is deduced from earthquake focal mechanism data (Zoback, 1992), mainly provided by the routinely determined Harvard centroid moment tensor (CMT) solutions (Dziewonski et al., 1987) and moment tensors by other institutions. Thus the distribution of WSM stress information reflects the global seismicity pattern (Fig. 1a).

Figure 1b shows the magnitude statistics of CMT-solutions determined per year since 1976. Below $M_w = 5.0-5.5$ the number of evaluated seismic events decreases significantly. Since earthquake magnitude statistics follow the logarithmic Gutenberg-Richter relation, the number of events $4.5 \leq M_w < 5.0$ per year for which no moment tensor solution is calculated is greater than 2000. Thus the determination of low magnitude earthquake focal mechanisms especially for intraplate regions of moderate seismicity holds a high potential of new stress information that can give important insights into active tectonics (Fan and Wallace, 1991) and detailed information in terms of seismic hazard assessment.

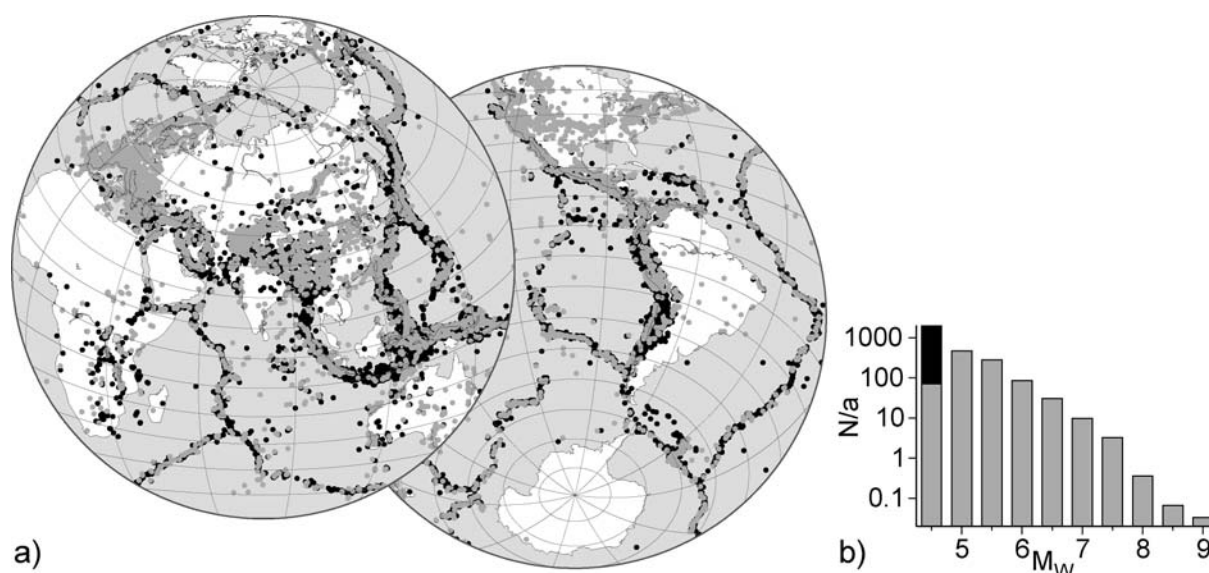


Figure 1: a) Global seismicity $M_w \geq 4.5$ (black dots, Engdahl et al., 1998) since 1996, overlaid by WSM data locations (grey dots). Accumulation of black symbols indicate intraplate regions of intermediate seismicity where only sparse stress information available. b) Number of CMT-solutions (grey bars) and events without source information (black) per year versus moment magnitude M_w .

We present a frequency sensitive moment tensor inversion that allows to determine low magnitude earthquake focal mechanisms using data from regional and teleseismic seismometers. Intraplate regions where only sparse stress information is available but intermediate seismicity is present are for example eastern Africa, inner Asia including the Baikal region and the inner Indo-Australian plate (Fig. 1a). As a case study we will determine new focal mechanism solutions for low magnitude events $M_w < 5.0$ in eastern Africa using the permanent seismometer network. Finally, we will combine the new mechanisms with CMT-solutions and other datasets to perform stress inversions for separate regions and discuss the results in terms of eastern African tectonics.

THE EAST AFRICAN RIFT SYSTEM

The East African Rift System (EARS) is a rare example of active continental rifting. Passing for nearly 3000 km through the continent, the EARS separates the Nubian subplate to the west from the Somalian subplate to the east (Fig. 2). Beginning on the Afar triple junction, it crosses the Ethiopian highland and leads to the eastern rift branch dispersing in northern Tanzania. Grimison and Chen (1988), however, proposed an extended eastern branch that connects to the Davie Ridge along the continental margin on the coast of eastern Africa, to explain the seismic activity in the northern Mozambique Channel. The western branch starts in southern Sudan and runs through the rift valley lakes to Mozambique, including Lake Tanganyika and Lake Malawi.

Source mechanisms in eastern Africa were examined by several studies using both first motion analysis (e.g. Fairhead and Girdler, 1971) and waveform inversion. Shudofsky (1985) used Rayleigh-waveform inversion to calculate source mechanisms for earthquakes with magnitudes $M_w \geq 5.0$ from the years 1964 to 1977. He obtained 23 focal mechanisms all over Africa and thus demonstrated the viability of this technique in a region of moderate seismicity and sparse data. Since 1977—the beginning of routine determination of the Harvard CMT's (Dziewonski et al., 1987)—90 focal mechanisms were given in the study region until end 2005 (CMT catalog, <http://www.globalcmt.org>). The global level of completeness for CMT-solutions is approximately $M_w \geq 5.5$ (Arvidsson and Ekström, 1998), whereas for eastern Africa the level of completeness is $M_w \geq 5.3$ (Barth, 2007), including events as low as $M_w = 4.7$. Thus for strong and most of moderate magnitude events the CMT-solution is given.

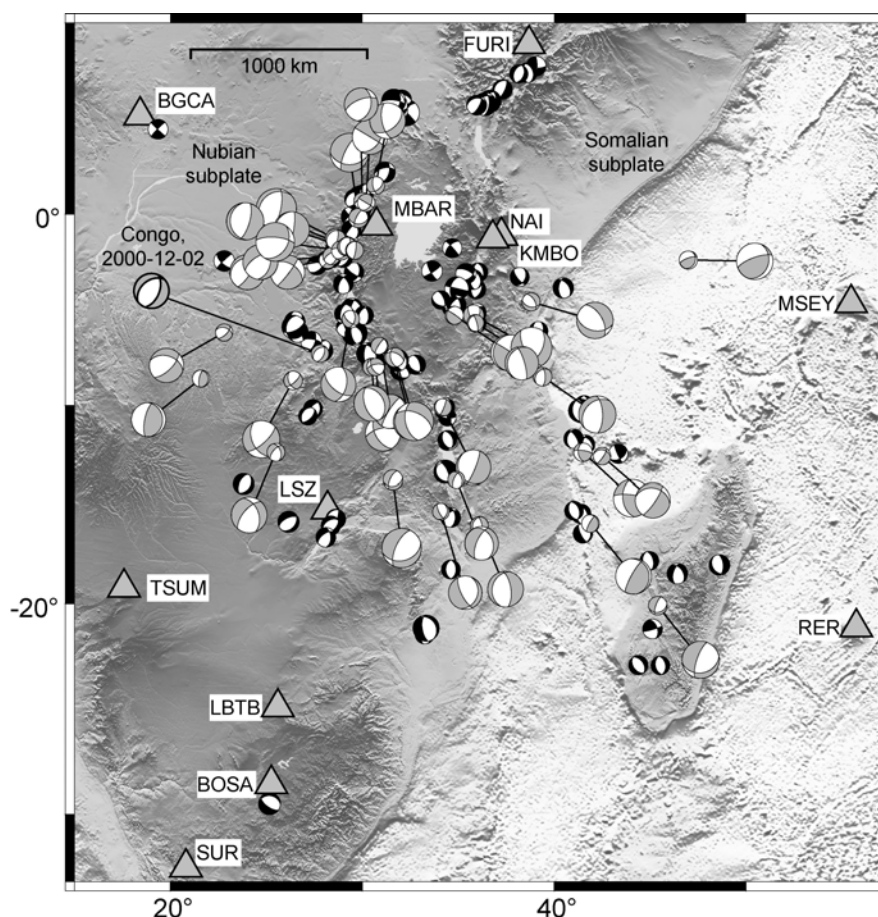


Figure 2: Result of the frequency sensitive moment tensor inversion showing the 38 newly determined focal mechanisms (large grey beach balls). Smaller black mechanisms are given by CMT-solutions and other publications (see text for references). Triangles indicate seismic stations.

FREQUENCY SENSITIVE MOMENT TENSOR INVERSION

Data

We use recordings of broadband and long-period seismometers with source-receiver distances up to 3300 km to investigate source mechanisms of earthquakes $M_w < 5.0$ in eastern Africa. Additionally, we restrict the moment tensor inversion to the times after 1995, for which sufficient data are available. We use seismic data of 13 seismometers receiving a good azimuthal distribution with respect to eastern Africa (Fig. 2). Waveform data of all stations are available online via the IRIS-datacenter Washington (<http://www.iris.edu/SeismiQuery>). Earthquake locations were taken from the Engdahl catalogue of relocated earthquakes (Engdahl et al., 1998) and only events are considered for that no Harvard CMT-solution was determined previously.

Frequency sensitive processing

We apply a damped least squares moment tensor inversion in the frequency-domain to fit the spectral amplitude pattern (Giardini, 1992; Bernardi et al., 2004). Synthetics are generated by normal mode summation (Woodhouse, 1988) for the one-dimensional PREM earth model (Dziewonski and Anderson, 1981), that makes the inversion routine easily transferable to regions worldwide. However, this restricts the inversion to long-period waves, that are less influenced by structural heterogeneities than short periods (Larson and Ekström, 2001). Šílený (2004) showed that periods $T \geq 35$ s are sufficient for the determination of moment tensors for low magnitude events using a one-dimensional earth

model. Beside this short-period limit, the usable waveform data are also limited for long-period waves. Low magnitude earthquakes provide amplitudes higher than the seismic noise level only at waves of rather short periods when recorded at teleseismic distances. Thus, for the moment tensor determination in regions of only intermediate seismicity and sparse seismometer coverage, source-relevant data of long-period waves ($T > 100$ s) disappear within the seismic noise. These two limits restrict the data used in this study to periods $T = 35-100$ s ($f = 10-29$ mHz). Harvard CMT-solutions are calculated automatically inverting long-period body and surface waves using two constant pass-bands of periods of $T > 45$ s respective $T > 135$ s recorded by permanent seismometers of the global network in teleseismic distances (Dziewonski et al., 1987). However, analysing low magnitude events with little seismic data the inverted frequency band of waveform data has to be chosen adequately in dependence of the earthquake magnitude and distribution of seismic stations, (Braunmiller et al., 2002). Since these effects have differing influences on the individual waveforms, a reliable waveform dataset has to be compiled to perform a stable earthquake source study. For this purpose we automatically invert the source-relevant long-period part of each waveform trace at first solely to determine waveforms with a high signal-to-noise ratio (Barth et al., 2007).

To account for these difficulties of source mechanism analysis we perform the frequency sensitive moment tensor inversion. The semi-automatic data processing follows a strict scheme and includes three steps: 1) Determination of an initial dataset N_{init} ; 2) Extraction of the final data set N_{final} in dependence on hypocentral depth and inverted frequency range; 3) Frequency sensitive analysis for the final dataset to determine the final frequency range F_{final} and the optimum hypocentral depth. Here we will give a short overview concerning the inversion procedure. A detailed description can be found in Barth et al. (2007).

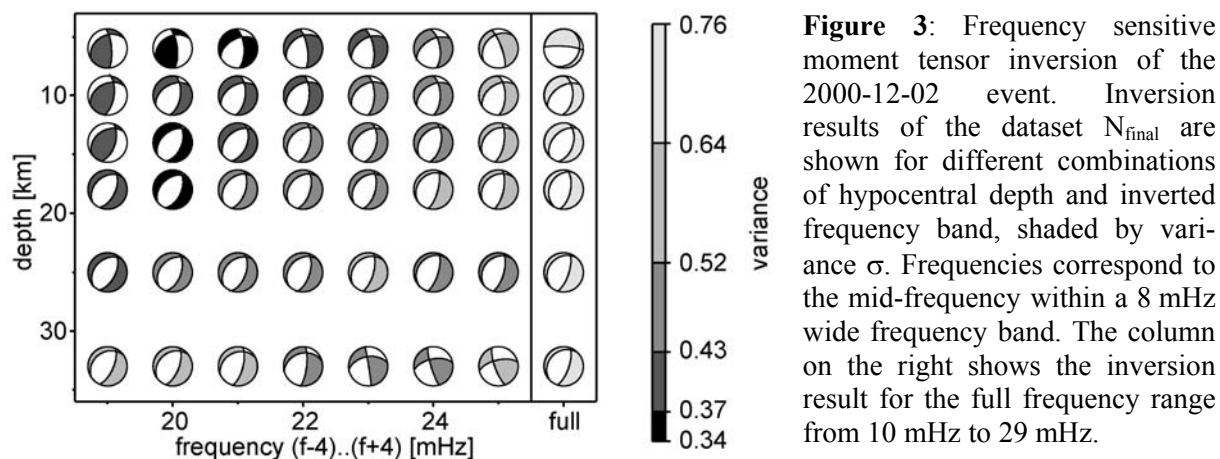
(Step 1) To determine the initial dataset N_{init} we invert each single waveform component for the moment tensor to decide whether its waveform could be explained by an arbitrary source mechanism and the one-dimensional earth model. The inversion is performed for a sliding 8 mHz wide frequency band between 8 mHz and 29 mHz and a constant hypocentral depth given by Engdahl et al. (1998). The moment tensor inversion minimises for the data variance σ between observed \mathbf{d} and synthetic waveforms \mathbf{s} :

$$\sigma = (\mathbf{d} - \mathbf{s})^2 / \mathbf{d}^2 . \quad (1)$$

To receive a robust initial dataset, we define limits for the data variance σ to separate explainable data and such biased by noise and effects of crustal complexity. Thus for each frequency range an initial dataset N_{init} is determined that only includes waveforms that result in variances below this limit. Finally, we take the initial dataset N_{init} for the frequency range with the largest number of high quality components and extend it to frequencies with a similarly high amount of explainable data.

(Step 2) Next we define the final dataset N_{final} by reducing N_{init} to the set of waveforms that could be explained by a common moment tensor: One by one the waveform explained worst is excluded from the dataset and the inversion is performed again until the waveform components for all stations have an individual variance below the threshold. Again this step is repeated for a sliding 8 mHz frequency band, but this time with discrete crustal source depths. This iterative procedure reduces N_{init} to an individual dataset for each depth-frequency combination. The dataset with the lowest variance σ is chosen as final waveform dataset N_{final} , whereas the according focal mechanism solution must be similar to the mechanisms of adjacent inverted frequencies. We define similarity of two focal mechanisms by an average difference in orientation of the principal axes of two moment tensors less than 30° (Bernardi et al., 2004).

(Step 3) As the previous steps are necessary to obtain the waveform dataset, we now perform the frequency sensitive inversion for the final dataset N_{final} . The inversion for the deviatoric moment tensor is applied for the discrete source depths by sliding frequency bands. The depth-frequency pair with the lowest variance is selected and the band-width extended to F_{final} , that is the widest range of



similar focal mechanisms. Finally, we determine the hypocentral depth with the lowest variance by inverting the fixed dataset N_{final} and frequency band F_{final} for the discrete source depths.

Inversion results

As described in Barth et al. (2007) we determined 38 reliable moment tensors for eastern Africa within the years 1995-2002 and moment magnitudes that range from M_W 4.4 to M_W 5.5 (median $M_W = 4.8$). The individual focal mechanism solutions are shown in Figure 2. As expected the majority of analysed events concentrates along the East African Rift System, but 13 moment tensors are determined for earthquakes in neighbouring regions. The predominant regime is normal faulting.

Congo - M_W 4.7 earthquake, 2000-12-02

A representative earthquake to demonstrate the frequency sensitive moment tensor inversion is the event of 2 December 2000, 04:16:43 UTC that occurred west of the western rift branch in the Democratic Republic of Congo at 7.3°S/27.8°E. The inversion is performed using ten waveform components of seven seismometers with source-receiver distances between 800 and 3100 km (Barth et al., 2007).

The frequency sensitive inversion of N_{final} for discrete source depths (step 3) is given in Figure 3. The inversion is performed for 8 mHz wide frequency pass-bands within the frequency range $F_{\text{init}} = 15$ -29 mHz and shows an area of similar and low variance normal faulting mechanisms for the central frequency bands. On the low-frequency edge mechanisms tend to flip into the opposite regime, whereas for high frequencies data variance increases. The depth-frequency combination with lowest variance is found at $F_{\text{final}} = 16$ -24 mHz for a source depth of 18 km. Similarly low variances result for shallower depths, while deeper origins can be excluded. To demonstrate the necessity of a frequency sensitive inversion we invert the dataset N_{final} for the full frequency band from 10 mHz to 29 mHz (Fig. 3, right column). Compared to the stable, low variance depth-frequency region inverted for the narrow frequency bands, variances for this rather wide frequency band are high and focal mechanisms are partly rotated (Barth et al., 2007). The inversion of N_{final} for F_{final} fits the surface wave-trains in phase and amplitude very well (Fig. 4) and results in a seismic moment of $1.36 \cdot 10^{16}$ Nm ($M_W = 4.7$). The solution shows a normal faulting mechanism, striking in northeast/southwest orientation. The nodal planes dip with 40° and 53°, respectively. The mechanism roughly agrees with Harvard CMT-solutions determined previously for that region (compare Fig. 2).

STRESS INVERSION

The formal stress inversion from focal mechanisms are based on following assumptions for the study region (Michael, 1984): (a) The stress field is uniform and invariant in space and time. (b) Earthquake slip occurs in direction of maximum shear stress (Wallace-Bott hypothesis, Bott, 1959).

DEMOCRATIC REP OF CONGO

Date: 2.12.0 Time: 4:16:43.0 Lat: -7.30 Long: 27.80 Depth: 18 Mw: 4.7
 Plane (strike/dip/slip) NP1: 230/40/-68 NP2: 22/53/-107 Variance: 0.348

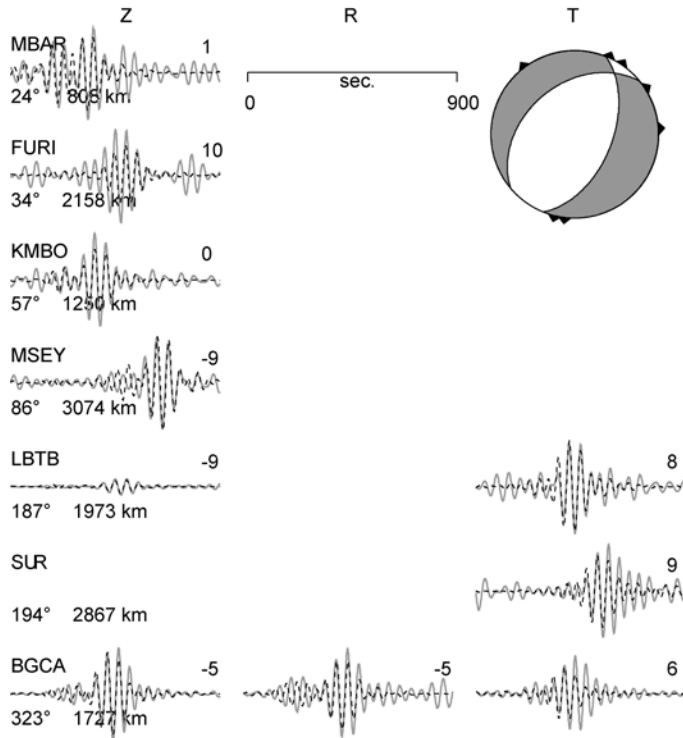


Figure 4: Final result of the moment tensor inversion of the 2000-12-02 event for the frequency range $F_{\text{final}} = 16\text{-}24$ mHz and a hypocentral depth of 18 km. Triangles around the focal mechanism indicate station azimuth. The inverted waveform traces N_{final} on the vertical, radial and transversal component (Z,R,T) are plotted as solid lines, synthetics as dashed lines. Station name is given above each trace, azimuth and epicentral distance below. Upper right numbers are time shifts in seconds applied to optimise the phase fit. Plotted amplitudes are normalised to the maximum of each station.

To take account of the ambiguity between focal and auxiliary plane of the source mechanism we apply a statistical approach, that inverts different combinations of fault planes to see which stress tensor is most likely. The composition of each dataset is twofold: At first a bootstrap routine is performed that picks n mechanisms at random from the original n events. Each dataset then will have some mechanisms repeated two or more times. Thereafter the fault plane is chosen randomly from the two auxiliary planes (Michael, 1987). Thus, several thousand synthetic datasets are compiled by one original set of focal mechanisms and inverted for the orientation of maximum shear stress. A statistical analysis then gives the best fitting stress orientation. Since this strategy does not decide for one fault plane and the dependence on individual focal mechanism solutions is decreased, this method is appropriate.

Focal mechanism solutions for eastern Africa

We combine the 38 newly determined focal mechanisms of this study with other mechanisms calculated by moment tensor inversion to invert for the regional stress field in eastern Africa (Fig. 2). The greatest number is taken from the Harvard-CMT catalogue that provides 90 focal mechanisms from 1977 until 2005 within the study region. Beside this, 17 additional provides mechanisms of strong events are given by four publications from 1964-1977 (all 17 by Shudofsky, 1985 and re-evaluations by Foster and Jackson, 1998 {5}; Grimison and Chen, 1988 {1} and Nyblade and Langston, 1995 {1}).

Zonation and resulting stress orientations

Since the focal mechanism data are not consistent for the inversion of entire eastern Africa and thus the misfit between orientation of maximum shear stress and slip direction is rather high (Barth, 2007), we divide the region into sub-areas to study regional changes in stress orientation. For this purpose the zonation of the Global Seismic Hazard Assessment Program (GSHAP) is applied. These worldwide zonations take into account the recent and historic seismicity and hence define areas with a common seismic risk (Giardini, 1999). Hereby, eastern Africa is divided into 21 areas from the Afar-region in the north to southern South Africa, eight of which are located in our study region (Midzi et al., 1999).

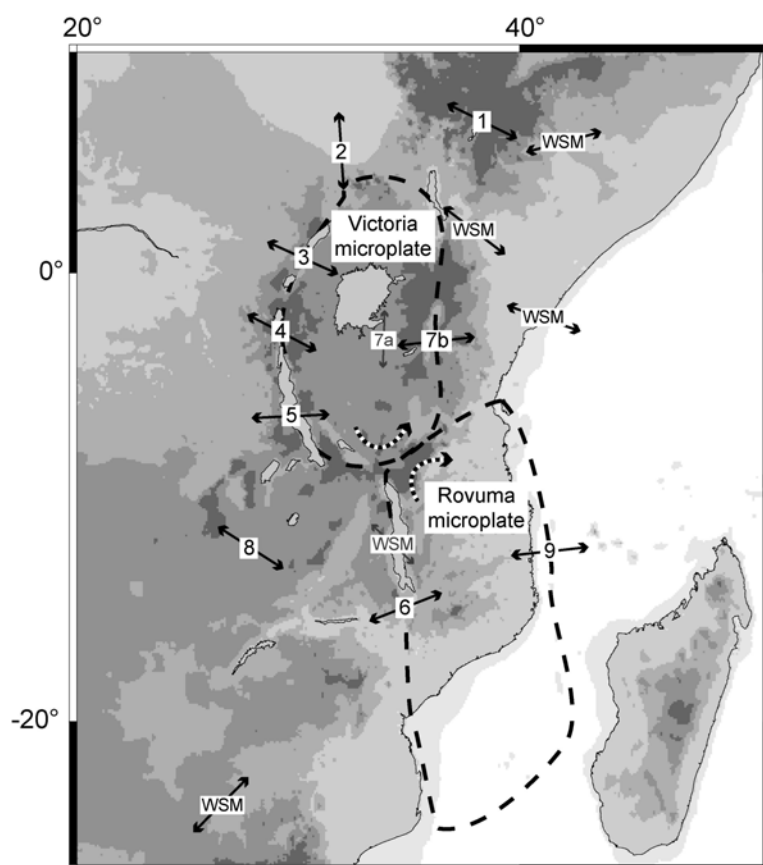


Figure 5: Orientation of minimum horizontal stress S_h from stress inversion in this study (numbers 1-9) and averaged WSM-data. Black pairs of arrows indicate reliable data, grey coloured pairs less reliable data. Dashed lines border the Victoria and Rovuma microplate with direction of rotation given by the black/white dashed arrows (Calais et al., 2006).

By this means, datasets of focal mechanism solutions are defined, for that the stress inversion can be performed. Since some events are not binned into one of the GSHAP-areas and some areas include up to 50 events, we adapt the GSHAP-classification to our dataset of 145 focal mechanisms. The inversions of these ten areas reveal a general trend of east/west extension (corresponding to the orientation of minimum horizontal stress S_h) all over eastern Africa (Fig. 5). Moreover a clear trend of changing stress pattern from northwest to southeast is obvious. While the northwestern segments of the EARS (areas 1,3-5) and the region south of it on the high plateau of Zambia and southern Congo (area 8) have extensional regimes with west-northwest/east-southeast orientation of S_h , the eastern rift branch (area 7b), the southernmost rift segment along Lake Malawi (area 6) and the continental margin including Madagascar (area 9) reveal a S_h orientation of east-northeast/west-southwest. Only the distinct areas along the Aswa fault-zone (area 2) and the area between the eastern rift branch and Lake Victoria (area 7a, high misfit) show north/south oriented extension (Barth, 2007).

DISCUSSION

Moment tensor inversion

The misfit between observed and calculated data in the frequency domain is given by the variance σ (Eq. 1), that is on average $\sigma = 0.41$ with $0.17 < \sigma < 0.71$ for the 38 moment tensor inversions (Barth et al., 2007). Compared with other studies the solutions provide a good fit (Bernardi et al., 2004). For the main part of the results variance σ increases with decreasing earthquake magnitude, since for weak events the amplitude of the seismic signals can be as low as the seismic noise level, hence biasing the transient wave signal. The generally low level of σ is obtained by systematically excluding waveform components with high variances by step 2 of the semi-automatic processing. In combination with the frequency sensitive analysis this allows the determination of source mechanisms for magnitudes as low as M_w 4.4 and thereby the decrement of the magnitude threshold of moment tensor inversion for eastern Africa from $M_w \sim 5.3$ (Harvard CMT-solutions) to $M_w \sim 5.0$ (Barth, 2007).

The relation between inverted frequency band and moment magnitude for the 38 moment tensor inversions shows that the high-pass frequency is lower for higher magnitudes, as described by previous studies (Braunmiller et al., 2002). The average number of inverted waveform traces per earthquake is nine with a maximum of 19 waveforms. Inverting less than six waveforms, the small amount of data can be fitted by various mechanisms, for structural heterogeneities could wrongly be mapped into the source process (Rao et al., 2002). This can lead to rotated beach balls when the frequency band is varied little, with small depth-frequency regions of stable focal mechanisms. Thus only earthquakes that provide a good signal-to-noise ratio for a sufficient amount of data are analysed. Since inversions for only six to eight waveforms do not result systematically in high variances the limit of six waveforms is an adequate restriction.

Eastern African stress pattern

The stress inversion reveals a general trend of east/west extension. Moreover, from northwest to southeast a smooth change from west-northwest/east-southeast to east-northeast/west-southwest extension is visible. Figure 5 shows averaged stress data contained in the World Stress Map (WSM) database (Müller et al., 2003; Reinecker et al., 2005), excluding focal mechanism data used in this study. Beside some overcoring data south of 20°S, where no focal mechanisms are known, borehole breakouts and data from geological field observations are available. Compared to the S_h orientations resulting from our stress inversion, the WSM-data partly support the stress change of S_h from northwest to southeast.

Coblentz and Sandiford (1994) showed by two-dimensional finite element modelling that first-order stress pattern are a mostly a consequence of differences in gravitational potential energy. However, their two-dimensional model cannot resolve a stress change as determined in this work, probably because the regional tectonics are mainly influenced by three-dimensional structures such as existing microplates. Calais et al. (2006) observed deviations in the direction of motion of microplates in eastern Africa. By GPS- and earthquake slip-data from CMT-solutions they concluded that the EARS consists of at least two distinct microplates named Victoria and Rovuma. The Victoria block is located around Lake Victoria south of the Aswa fault-zone between the eastern and western rift branch. The Rovuma block between the Lake Malawi and the Davie Ridge borders in the north on the Victoria block. An opposite rotation of these two microplates (Victoria counter-clockwise, Rovuma clockwise), as proposed by Calais et al. (2006) influenced by local mantle up-wellings could possibly explain the spatially changing stress field.

CONCLUSIONS

For the case study of eastern Africa we determined 38 focal mechanisms with $M_w = 4.4-5.5$ for source-receiver distances up to 3300 km. The investigation of focal mechanisms of low magnitude earthquakes calculated from sparse teleseismic waveform data reveals a strong dependence on the inverted frequency pass-band. To take into account this dependence, we developed an iterative and frequency sensitive processing to perform the moment tensor inversion. This semi-automatic procedure determines a dataset of high quality waveform data, the maximum width frequency pass-band of similar and low variance moment tensors and the hypocentral depth. Thus, all determined moment tensors have low variances and are stable within the finally inverted frequency band. We inverted only waveforms with periods longer than 35 s that are less affected by structural heterogeneities than short period waves and only periods shorter than 100 s, since source-relevant data of long-period waves ($T > 100$ s) disappear within the seismic noise.

The separate stress inversions for ten distinct areas result in a prevailing extensional stress regime in eastern Africa with predominantly east/west oriented S_h . Beyond this, the orientation of S_h changes from west-northwest/east-southeast in the northwest to east-northeast/west-southwest in the southwest of the study region. While the first-order pattern of east/west extension in eastern Africa can be explained by the effect of gravitational potential energy differences (Coblentz and Sandiford, 1994), a possible reason for the stress change is probably related to the existence the two microplates Victoria

and Rovuma, that are located between the Nubian and Somalian subplate. Hence, local mantle upwellings could be the reason for the spatial changes in the stress field around these microplates and their opposite rotation, as constrained by GPS-data (Calais et al., 2006).

We have shown that even with a sparse teleseismic station distribution moment tensor inversion of earthquakes with $M_w < 5.0$ is possible. By using a one-dimensional earth model (Dziewonski and Anderson, 1981) and waveform data of the permanent global seismometer network, the described processing is easily transferable to other regions of intermediate seismicity. Thus frequency sensitive moment tensor inversion has a high potential of enlarging the number of calculated focal mechanism solutions worldwide to increase the global stress information and improve the understanding of regional tectonics.

ACKNOWLEDGMENTS

The seismic waveforms were provided by the networks of GEOFON, GEOSCOPE, GSN and GTSN, available online via the IRIS-datacenter Washington (<http://www.iris.edu/Seismi-Query/>). Seismic data was processed with SeismicHandler (Stammler, 1993) and inverted for the moment tensor by the gminl-software (Giardini, 1992). The majority of the figures were made using GMT (Wessel and Smith, 1998).

REFERENCES

1. Arvidsson, R. and Ekström, G. (1998). Global CMT analysis of moderate earthquakes, $M_w \geq 4.5$, using intermediate-period surface waves. *Bull. Seism. Soc. Am.*, **88**(4):1003–1013.
2. Barth, A., 2007. Frequency sensitive moment tensor inversion for light to moderate magnitude earthquakes in eastern Africa and derivation of the regional stress field, Ph.D. Thesis, University of Karlsruhe, Germany.
3. Barth, A., Wenzel, F. and Giardini, D. (2007). Frequency sensitive moment tensor inversion for light to moderate magnitude earthquakes in Eastern Africa, in prep.
4. Bernardi, F., Braunmiller, J., Kradolfer, U., and Giardini, D. (2004). Automatic regional moment tensor inversion in the European-Mediterranean region. *Geophys. J. Int.*, **157**:703–716.
5. Bott, M. H. P. (1959). The mechanics of oblique slip faulting. *Geol. Mag.*, **96**(2):109–117.
6. Braunmiller, J., Kradolfer, U., Baer, M., and Giardini, D. (2002). Regional moment tensor determination in the European-Mediterranean area - initial results. *Tectonophysics*, **356**:5–22.
7. Calais, E., Hartnady, C., Ebinger, C., and Nocquet, J. M. (2006). Kinematics of the East African Rift from GPS and earthquake slip vector data. In Yirgu, G., Ebinger, C. J., and Maguire, P. K. H., editors, *Structure and Evolution of the Rift Systems within the Afar volcanic province, Northeast Africa*, **259**:9–22. *Geol. Soc. Lond. Spec. Publ.*
8. Coblenz, D. D. and Sandiford, M. (1994). Tectonic stresses in the African plate: Constraints on the ambient lithospheric stress state. *Geology*, **22**:831–834.
9. Dziewonski, A. M. and Anderson, D. L. (1981). Preliminary reference earth model. *Phys. Earth Planet. Int.*, **25**(4):297–356.
10. Dziewonski, A. M., Ekström, G., Franzen, J. E., and Woodhouse, J. H. (1987). Global seismicity of 1977: Centroid-moment tensor solutions for 471 earthquakes. *Phys. Earth Planet. Int.*, **45**(1):11–36.
11. Engdahl, E. R., van der Hilst, R., and Buland, R. (1998). Global teleseismic earthquake relocation with improved travel times and procedures for depth determination. *Bull. Seism. Soc. Am.*, **88**(3):722–743.
12. Fairhead, J. D. and Girdler, R. W. (1971). Seismicity of Africa. *Geophys. J. Roy. Astr. Soc.*, **24**(3):271–301.
13. Fan, G. and Wallace, T. (1991). The determination of source parameters for small earthquakes from a single, very broadband seismic station. *Geophys. Res. Lett.*, **18**(8):1385–1388.
14. Foster, A. N. and Jackson, J. A. (1998). Source parameters of large African earthquakes: Implications for crustal rheology and regional kinematics. *Geophys. J. Int.*, **134**:422–448.

15. Giardini, D. (1992). Moment tensor inversion from mednet data - large worldwide earthquakes of 1990. *Geophys. Res. Lett.*, **19**(7):713–716.
16. Giardini, D. (1999). The global seismic hazard assessment program (GSHAP)1992/1999. *Ann. Geofis.*, **42**(6):957–974.
17. Grimison, N. L. and Chen, W. P. (1988). Earthquakes in the Davie Ridge Madagascar region and the southern Nubian Somalian plate boundary. *J. Geophys. Res.*, **93**(B9):10439–10450.
18. Heidbach, O., Barth, A., Connolly, P., Fuchs, K., Müller, B., Tingay, M., Reinecker, J., Sperner, B., and Wenzel, F. (2004). Stress maps in a minute: The 2004 World Stress Map release. *Eos, Trans. AGU*, **85**(49):521.
19. Larson, E. W. F. and Ekström, G. (2001). Global models of surface wave group velocity. *Pure Appl. Geophys.*, **V158**(8):1377–1399.
20. Michael, A. J. (1984). Determination of stress from slip data: Faults and folds. *J. Geophys. Res.*, **89**(B13):11,517–11,526.
21. Michael, A. J. (1987). Use of focal mechanisms to determine stress: A control study. *J. Geophys. Res.*, **92**(B1):357–368.
22. Midzi, V., Hlatywayo, D. J., Chapola, L. S., Kebede, F., Atakan, K., Lombe, D. K., Turyomurugyendo, G., and Tugume, F. A. (1999). Seismic hazard assessment in eastern and southern Africa. *Ann. Geofis.*, **42**:1067–1083.
23. Müller, B., Wehrle, V., Hettel, S., Sperner, B., and Fuchs, K. (2003). A new method for smoothing oriented data and its application to stress data. In Ameen, M., editor, *Fracture and in-situ stress characterisation of hydrocarbon reservoirs*, **209**:107–126. *Geol. Soc. Lond. Spec. Publ.*
24. Nyblade, A. A. and Langston, C. A. (1995). East-African earthquakes below 20-km depth and their implications for crustal structure. *Geophys. J. Int.*, **121**(1):49–62.
25. Rao, N. P., Tsukuda, T., Kosuga, M., Bhatia, S. C., and Suresh, G. (2002). Deep lower crustal earthquakes in central India: Inferences from analysis of regional broadband data of the 1997 May 21, Jabalpur earthquake. *Geophys. J. Int.*, **148**:132–138.
26. Reinecker, J., Heidbach, O., Tingay, M., Sperner, B., and Müller, B. (2005). The release 2005 of the World Stress Map (available online at <http://www.world-stress-map.org>).
27. Shudofsky, G. N. (1985). Source mechanisms and focal depths of East African earthquakes using Rayleigh-wave inversion and body-wave modelling. *Geophys. J. Roy. Astr. Soc.*, **83**:563–614.
28. Šílený, J. (2004). Regional moment tensor uncertainty due to mismodeling of the crust. *Tectonophysics*, **383**:133–147.
29. Stammer, K. (1993). SeismicHandler: Programmable multichannel data handler for interactive and automatic processing of seismological analyses. *Comp. Geosci.*, **19**:135–140.
30. Wessel, P. and Smith, W. H. F. (1998). New, improved version of Generic Mapping Tools released. *Eos, Trans. AGU*, **79**:579pp.
31. Woodhouse, J. H. (1988). The calculation of eigenfrequencies and eigenfunctions of the free oscillations of the earth and the sun. In Doornbos, D. J., editor, *Seismological Algorithms*, 321–370. Academic Press, London.
32. Zoback, M. L. (1992). First- and second-order patterns of stress in the lithosphere: The World Stress Map project. *J. Geophys. Res.*, **97**(B8):11,703–11,728.